Article

Research on Enhancement of LIBS Signal Stability Through the Selection of Spectral Lines Based on Plasma Characteristic Parameters

Yunfeng Xia [1], Honglin Jian [2], Qishuai Liang [1] and Xilin Wang [2],*

[1] Transmission Operation & Maintenance Branch of Hainan Power Grid Corporation, China Southern Power Grid Co., Ltd., Haikou 570000, China; xyf0725@163.com (Y.X.); 18976002594@163.com (Q.L.)

[2] Shenzhen International Graduate School, Tsinghua University, Shenzhen 518000, China; jianhl23@mails.tsinghua.edu.cn

* Correspondence: wang.xilin@sz.tsinghua.edu.cn

Abstract: Laser-induced breakdown spectroscopy (LIBS) is widely used for online quantitative analysis in industries due to its rapid analysis and minimal damage. However, challenges like signal instability, matrix effects, and self-absorption hinder the measurement accuracy. Recent approaches, including the internal standard method and crater limitation method, aim to improve the stability but suffer from high computational demands or complexity. This study proposes a method to enhance LIBS stability by utilizing craters formed from laser ablation without external cavity assistance. It first improves the plasma temperature calculation reliability using multiple elemental spectral lines, after which electron density calculations are performed. By fitting plasma parameter curves based on laser pulse counts and using a laser confocal microscope for crater analysis, stable plasma conditions were found within crater areas of 0.400 mm^2 to 0.443 mm^2 and depths of 0.357 mm to 0.412 mm. Testing with elemental spectral lines of Ti II, K II, Ca I, and Fe I showed a significant reduction in the relative standard deviation (RSD) of the LIBS spectral line intensity, demonstrating an improved signal stability within specified crater dimensions.

Keywords: laser-induced breakdown spectroscopy; plasma temperature; electron density; stability

1. Introduction

In recent years, laser-induced breakdown spectroscopy (LIBS) [1] has gained significant attention from researchers due to its numerous advantages, such as minimal damage to materials, low detection limits, high sensitivity, real-time detection capabilities, and wide applicability in various fields including industry [2], agriculture [3], environmental protection [4], biomedicine [5], archaeology [6], and space exploration [7]. This technology generates plasma through laser ablation of the sample surface, and, during the cooling process of the plasma, characteristic spectra are emitted due to electronic transitions. The types and amounts of elements are analyzed through the wavelengths and intensities of the characteristic spectral lines.

However, this technology is not without its drawbacks. The signal is unstable due to fluctuations in laser parameters, and there are also influences from matrix effects and self-absorption effects, which lead to poor measurement stability in LIBS technology, severely limiting its field applications. Currently, many researchers are attempting to improve the measurement stability of LIBS technology through various methods, which can be mainly

categorized into data processing methods and experimental methods. Data processing primarily includes the optimization of experimental parameters, spectral line intensity normalization, internal standard methods, and reference signal correction methods. Zhu et al. [8] explored the effect of the gas temperature on LIBS in gas composition measurements. The results indicated that with an optimized gate width and delay time, as the gas temperature increased from 300 K to 930 K, the LIBS measurement error was approximately 5%, with an error of about 0.8% for every 100 K increase. Liu and colleagues [9] investigated the effect of environmental humidity on the LIBS of copper samples. The results indicated that at low laser energies (8 mJ and 13 mJ) the intensity of Cu I 510.55 nm decreased with increasing humidity, whereas at high laser energies (18 mJ, 30 mJ, and 50 mJ), the intensity increased with the humidity. The normalization method for the spectral line intensity utilizes the intensity of the entire spectrum or specific wavelength range to compensate for fluctuations in characteristic spectral lines, aiming to reduce the uncertainty of LIBS measurement signals, primarily relying on empirical approaches. Karki et al. [10] analyzed internal normalization, total light normalization, and background normalization, as well as their three-point smoothing methods, in the context of LIBS for the quantitative analysis of chromium (Cr), manganese (Mn), and nickel (Ni) in stainless steel. The results indicated that the internal normalization technique produced the best analytical results, followed by total light normalization. The internal standard method [11] compensates for fluctuations in plasma characteristics that affect measurements by selecting stable elements for internal calibration. However, the selection criteria are stringent, which increases the sample preparation time and limits practical applications. Pan et al. [12] proposed a multi-line internal standard calibration method for the quantitative analysis of carbon steel using LIBS. The results indicated that after employing the multi-line internal standard calibration method, all parameters showed a significant improvement, allowing for the effective acquisition of accurate and stable calibration curves.

Experimental methods include long and short dual-pulse techniques [13], varying ambient gas methods [14], pit restriction methods [15], and reference signal calibration methods [16]. The reference signal correction method utilizes signals generated during the plasma production process, such as plasma parameters, acousto-optic signals, and current signals, to correct the spectral line intensity. These methods involve significant computational effort and complex calculation processes. Wang Z and colleagues [17] improved a spectral normalization method applied to the measurement of copper (Cu) in 29 types of brass alloy samples, demonstrating enhancements in the measurement precision and accuracy compared to commonly used normalization methods. The long–short pulse method utilizes long-pulse lasers to sustain the plasma generated by short-pulse lasers, resulting in a more stable temperature and signal, an extended plasma lifetime, and an increased plasma volume, though it poses technical challenges in operation. Elnasharty et al. [18] utilized collinear double-pulse laser-induced breakdown spectroscopy (DP-LIBS) with microjoule nanosecond pulses, significantly enhancing the intensity and repeatability of emission signals in the elemental analysis of aluminum alloys. Hussain A et al. [19] studied the enhancement effects of magnetic field confinement and dual-pulse LIBS techniques on aluminum target plasma signals, finding that both significantly improved the spectral intensity and plasma parameters, with the dual-pulse technique showing a more pronounced enhancement effect. Another common experimental approach is the method of altering the ambient gas, which achieves a reduced relative standard deviation (RSD) by modifying the experimental environment. Jogi and colleagues [20] investigated the effects of nitrogen, argon, and helium on the detection of hydrogen isotopes in LIBS under atmospheric pressure. The study found that helium is the most favorable ambient gas for the LIBS detection of hydrogen isotopes at atmospheric pressure. Song YZ et al. [21] were the first to explicitly

reveal the mechanisms by which the primary properties of ambient gases (specific heat ratio, molar mass, and ionization energy) influence LIBS signals. They discovered that these properties determine the signal intensity and repeatability by affecting the plasma evolution and energy transfer processes, providing important references for plasma evolution studies and precise quantitative analysis in LIBS technology. The sample rotation method is commonly used in laboratories to improve the repeatability of LIBS measurements. Similarly, the cavity confinement method enhances and stabilizes LIBS signals by utilizing spatial confinement effects. The principle of the cavity confinement method is that the plasma generated by the laser in a confined space produces shock waves. When these shock waves contact the cavity walls, they reflect, thereby stabilizing the plasma and reducing signal fluctuations. These reflected shock waves further compress the plasma, increasing the collision frequency among particles, which, in turn, raises the temperature and electron density, ultimately enhancing the spectral signal. Therefore, the cavity confinement method improves the stability of LIBS measurements by influencing the state of the plasma, which can be reflected through the temperature and electron density. Wang et al. [22] significantly improved the signal intensity of LIBS by selecting appropriate diameters and materials for the cylindrical cavities, finding that an aluminum cavity with a diameter of 4 mm provided the best enhancement. Li et al. [23] studied the femtosecond laser-induced copper plasma constrained by spatial limitations within a cylindrical cavity, discovering that the emission intensity and spectral line lifetime of Cu atoms were significantly enhanced when using a cylindrical cavity with an inner diameter of 6 mm. The key to the pit restriction method lies in selecting the appropriate cavity size, as both excessively large and small cavities can affect the state of the plasma and the stability of the LIBS test signals, necessitating continuous experimentation with different cavity sizes in practical applications.

Inspired by the concept of the pit limitation method, we propose a technique to enhance the stability of LIBS signals by utilizing pits formed through laser ablation. Based on the variation patterns of plasma characteristic parameters (such as plasma temperature and electron density) with the number of laser pulses, we determined the specific number of laser pulses corresponding to a significant improvement in the LIBS signal stability. Using laser confocal technology, we measured the dimensions of the ablation pits at this point. By conducting a comparative analysis of the RSD of spectral lines for four elements under different pulse counts, the results demonstrate that the RSD of LIBS spectral lines is significantly reduced using our proposed method. This approach effectively determines the improvement in LIBS signal stability at specific pulse counts by leveraging pits formed through laser ablation and the trends in plasma parameters. Compared to existing experimental methods, this technique does not require additional laboratory equipment or complex operations, offering notable advantages such as a low cost and ease of on-site application. However, due to differences in the thermal properties, ionization energy, spectral band energy, and plasma behavior in complex chemical reactions of various materials, selecting parameters during experiments poses certain challenges, making it difficult to fully standardize the experimental conditions. Nevertheless, based on the method adopted in this study, the optimal experimental parameters can be determined simply and accurately, effectively addressing these differences and challenges.

2. Materials and Methods

2.1. Sample

The material used in this article was a white SMC high-pressure insulating board, purchased from Zhejiang Haodesheng Insulation Materials Co., Ltd. in Quzhou, China. This material is a composite that exhibits excellent electrical insulation properties, with high temperature and high pressure resistance, primarily composed of unsaturated resin

and fiberglass. The dimensions of the sample were 80 mm × 15 mm × 4 mm. The Energy Dispersive Spectroscopy (EDS) detection results of the samples are shown in Table 1. The samples contained various elements including C, O, Na, Mg, Al, Si, S, Cl, K, and Ca, among which Pt was introduced during the sample preparation for EDS detection.

Table 1. EDS test results for test samples.

Species	Element Content (%)
C	42.08
O	37.05
Na	0.30
Mg	0.52
Al	9.07
Si	3.98
S	0.07
Cl	0.11
K	0.19
Ca	4.43
Ti	0.88
Fe	0.31
Pt	1.02

2.2. Equipment

A schematic diagram of the LIBS system is shown in Figure 1, primarily consisting of a laser, digital delay generator, spectrometer, optical path, and fiber optic probe [24]. The laser used in the experiment was a nanosecond Nd:YAG laser model Nimma-900 from Leibao Photoelectric Company (Beijing, China), with the selected laser wavelength being 1064 nm. This wavelength exhibits good energy stability and has low attenuation in air. The digital delay generator was an eight-channel digital delay generator DG645 from Stanford Research Systems (Sunnyvale, CA, USA), with a delay resolution of 5 ps for all channels, with jitter between channels being less than 25 ps, and a delay control accuracy of 1 ns. This delay generator was utilized to set the timing for the laser and spectrometer, sending the Q-switch signal for the laser and the external trigger signal for the spectrometer to control the timing sequence. The spectrometer was the AVS-RACKMOUNT-USB2 from Beijing Avantes Co., Ltd. (Beijing, China), with a wavelength range of 200 nm to 640 nm and a resolution of 0.09 to 0.13 nm. The spectral integration time used in this study was 30 μs.
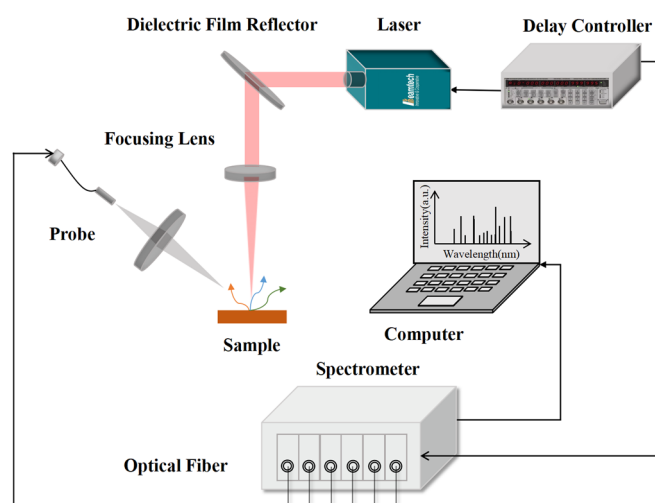

Figure 1. Schematic diagram of the LIBS system.

In the optical path, a dielectric mirror is a type of plane mirror that can efficiently reflect incident laser light of specific wavelengths while allowing good transmission of signals in the visible light spectrum. After passing through the dielectric mirror, the laser is focused onto the sample surface using a convex lens with a focal length of 110 mm. When the laser is focused on the sample surface, the energy density reaches the material's ablation threshold, generating plasma on the sample surface. After the plasma is formed, it expands under high temperature, and the temperature of the plasma gradually decreases. During this cooling process, the electrons in the plasma undergo transitions and emit characteristic spectral signals corresponding to the elements in the sample. To capture these spectral signals, a convex lens with a focal length of 60 mm is used in the optical path to focus the light emitted by the plasma onto the position of the light probe. The spectral signals collected by the light probe are then transmitted to a spectrometer from Beijing Avantes Co., Ltd. (Beijing, China) for processing and analysis via a computer.

2.3. Data Processing

The original spectrum is shown in Figure 2a. To eliminate the effects of fluctuations in parameters such as pulse energy and measurement efficiency, and to reduce matrix effects, the original spectrum was first subjected to area normalization. Next, baseline correction and noise reduction were performed on the normalized spectrum using discrete wavelet transform, resulting in the processed spectrum, as shown in Figure 2b. Subsequently, peak detection was conducted using continuous wavelet transform to identify valid spectral peaks for elemental matching. Finally, by referencing the Atomic Spectra Database (ASD) of the National Institute of Standards and Technology (NIST) [25], the central wavelengths of the test spectral peaks were compared with the standard wavelengths in the database to determine the elemental attribution of the spectral lines.
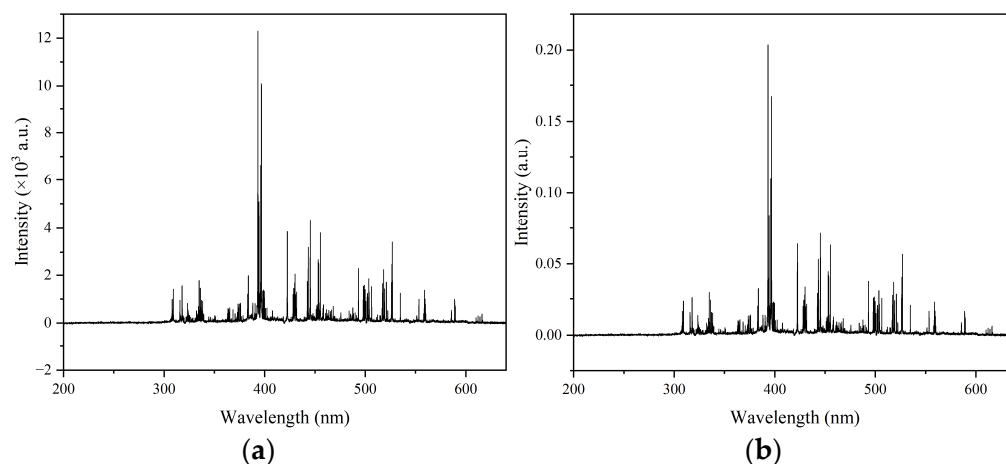

Figure 2. (**a**) Original spectrum graph. (**b**) Baseline-corrected and denoised spectrum.

The results of the primary element identification are shown in Figure 3. Four spectral lines with relatively high intensity and representative characteristic spectra were selected for analysis: Ti II 334.940 nm, K II 338.486 nm, Ca I 445.478 nm, and Fe I 455.445 nm.
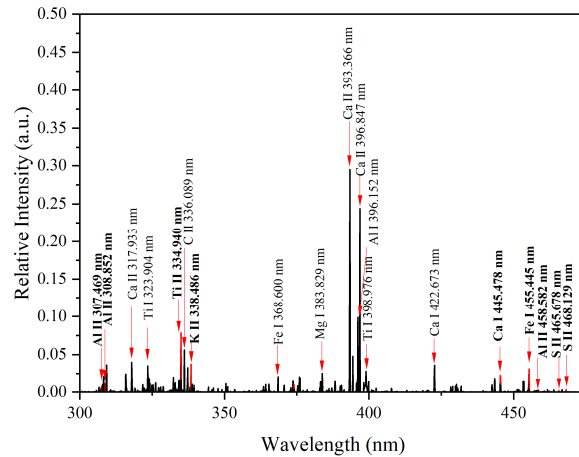
Figure 3. Identification results of the main elements in the LIBS spectrum from 300 nm to 470 nm.

2.4. System Parameter Optimization

Prior to the formal experiment, it was necessary to optimize the equipment parameters to ensure the acquisition of high-quality spectral information. First, at a single-pulse laser energy of 35 mJ, the spectrometer's light collection delay times were adjusted to 0.5, 1, 1.5, 2, 2.5, 3, 3.5, 4, 4.5, 5, 7, and 10 µs. Each delay time group underwent 10 tests to compute the average spectrum, thereby determining the signal-to-noise ratio, signal-to-background ratio, and spectral line intensity, as illustrated in Figure 4. Greater values of the signal-to-noise ratio, signal-to-background ratio, and spectral line intensity indicate better spectral information; thus, this study selected a delay time of 1.5 µs. The LIBS signal exhibited higher intensity at a 1.5 µs delay, which is related to the plasma evolution process. At 1.5 µs, due to the decay of background radiation and the excitation radiation reaching a stronger level, the signal intensity, signal-to-noise ratio, and signal-to-background ratio all improved.
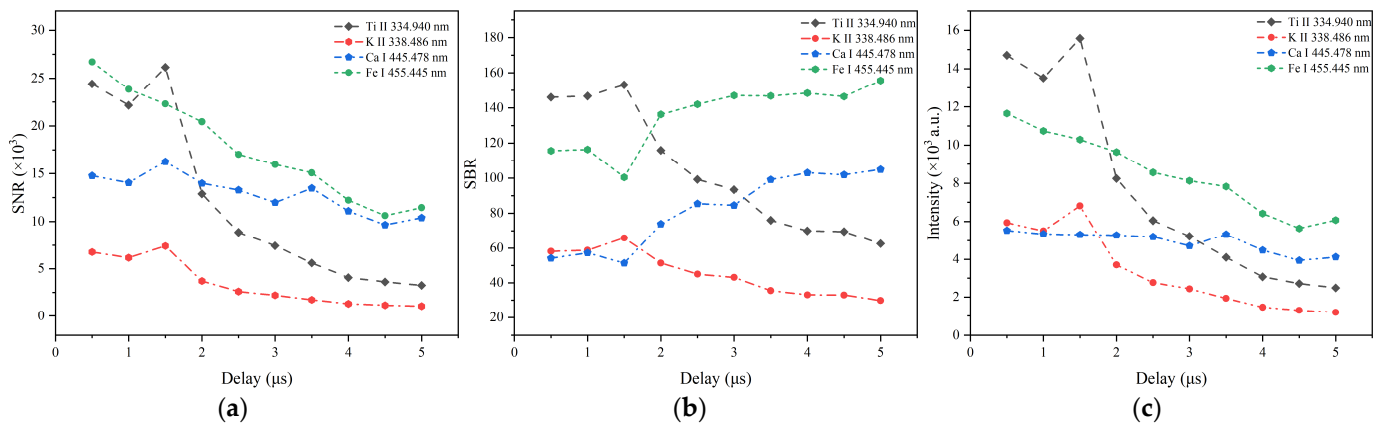

Figure 4. Variation in spectral parameters with delay time: (**a**) change in characteristic spectral line SNR with delay time; (**b**) change in characteristic spectral line SBR with delay time; (**c**) change in characteristic spectral line intensity with delay time.

After determining the delay time, further testing of the single-pulse laser energy was conducted, setting the energy levels to 35, 45, 55, 65, 75, 85, and 95 mJ. Similarly, each energy level was tested 10 times to obtain the signal-to-noise ratio, signal-to-background ratio, and spectral line intensity, as shown in Figure 5. Ultimately, a single-pulse laser energy of 95 mJ was chosen.
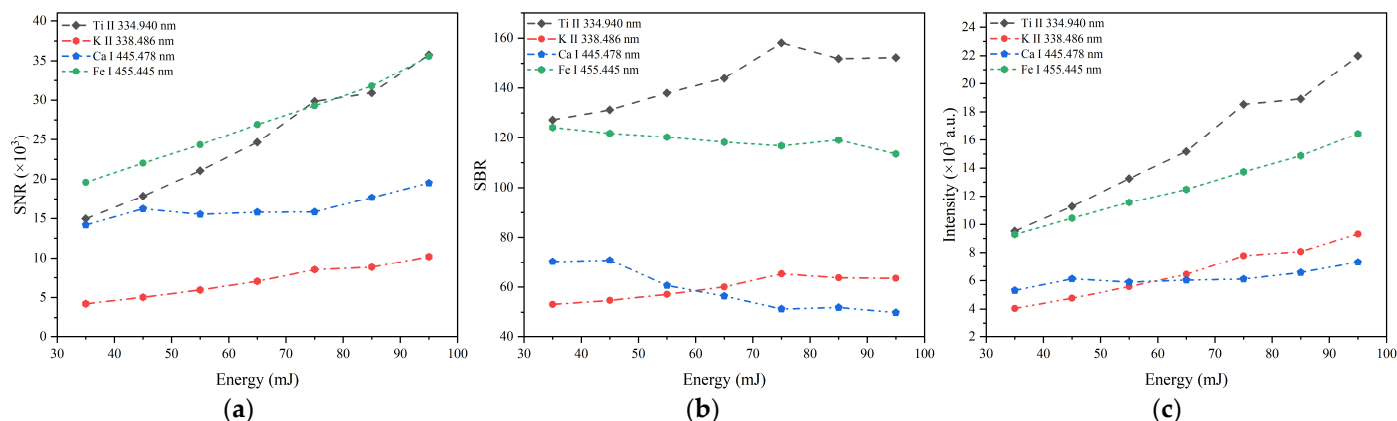
Figure 5. Variation in spectral parameters with single laser pulse energy: (**a**) change in characteristic spectral line SNR with single laser pulse energy; (**b**) change in characteristic spectral line SBR with single laser pulse energy; (**c**) change in characteristic spectral line intensity with single laser pulse energy.

3. Results

3.1. Plasma Parameters

The state of laser-induced plasma evolves rapidly, with its temperature and electron density also changing quickly. This rapid evolution significantly impacts the repeatability and accuracy of LIBS signals. By calculating the plasma temperature and electron density, a general understanding of the transient state of the plasma can be obtained [26]. Therefore, this study first focused on the calculation of the plasma temperature and the electron density.

According to Einstein's radiation theory, when plasma is in a state of local thermodynamic equilibrium (LTE), and without considering the effects of self-absorption, its spectral line intensity can be expressed as

$$I_{ij} = FN\frac{g_i A_{ij}}{Us(T)}e^{-\frac{E_i}{k_B T}} \tag{1}$$

where F is a constant determined using the experimental environment and system parameters, N denotes the particle number density, g_i represents the statistical weight of the high energy level i, and A_{ij} is the coefficient of spontaneous emission for the element. E_i is the excitation energy of energy level i, representing the degeneracy of the energy level i; k_B is the Boltzmann constant, approximately 1.38×10^{-23} J/K; T is the excitation temperature of the plasma; and $U_S(T)$ is the partition function. These parameters can be obtained from the NIST database. Furthermore, taking the logarithm of both sides of the above equation, it can be transformed into the following expression [27]:

$$\ln\frac{I_{ij}}{g_i A_{ij}} = \frac{-E_i}{k_B T} + \ln\frac{FN}{Us(T)} \tag{2}$$

Consider Equation (2) as a linear function, where the left side equals y and E_i equals x; thus, the plasma temperature T can be determined through the slope.

For different spectral lines, due to variations in parameters, there are different x and y values. By selecting multiple spectral lines of a specific element to obtain their x and y values, and performing linear fitting to determine the slope k, the plasma temperature T can be calculated. When selecting spectral lines, it is advisable to prioritize those with a larger difference in upper energy levels to achieve more accurate results.

In this study, a total of eight spectral lines of different elements (S and Al) was selected. The relevant information for these spectral lines is shown in Table 2. The energy levels of these spectral lines differ significantly, which is crucial for determining the plasma temperature. The plasma temperature was calculated using the ionic spectral lines of S and Al elements, and the final plasma temperature was obtained by averaging their calculated values. Figure 6 shows the fitting graph of the plasma temperature calculation from a particular test. It can be seen that the goodness of fit (R^2) for the S and Al element fitting curves was 0.9862 and 0.9610, respectively, both of which are close to 1, indicating a good fit. The plasma temperatures calculated using the S and Al spectral lines were 3938.5 K and 3625.4 K, respectively. The obtained plasma temperatures are relatively close, and the final plasma temperature was taken as their average value, 3781.95 K.

Table 2. Information on spectral lines used to determine plasma temperature.

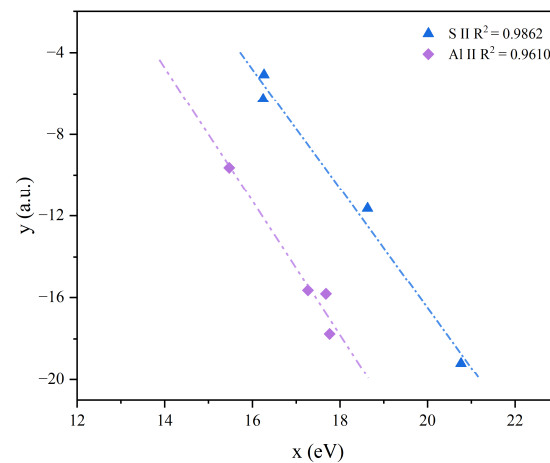| Species	Wavelength/nm	$A_{ki}/10^8$ s^{-1}	E_k/cm^{-1}	g_i
S II	374.116	7.19×10^7	167,472.42	4
S II	465.678	1.14×10^7	131,028.85	4
S II	468.129	4.12×10^5	131,187.19	6
S II	488.367	9.10×10^6	150,258.51	2
Al II	307.469	9.02×10^6	142,604.05	7
Al II	308.852	1.08×10^7	139,289.15	5
Al II	458.582	1.00×10^7	143,283.75	9
Al II	559.330	9.26×10^7	124,794.13	5

Figure 6. Schematic diagram for plasma temperature calculation.

In laser-induced plasma, the electron number density can be calculated using Stark broadening [28].

$$\Delta\lambda_{1/2} = 2\omega(N_e/10^{16}) \tag{3}$$

In the formula, w represents the electron collision parameter, and it can be obtained from the Stark database [29], where at 3781.95 K w is approximately 1.62×10^{-6} Å. $\Delta\lambda_{1/2}$ denotes the full width at half maximum of the spectral line. The Ca I 396.855 nm spectral line was selected as it is relatively independent and does not exhibit self-absorption phenomena. It has a well-defined profile, and through Lorentz fitting the full width at half maximum was obtained to calculate the electron number density. Figure 7 illustrates the Lorentz fitting results for the Ca I 396.855 nm spectral line from the same LIBS test as that used for calculating the plasma temperature mentioned earlier. The coefficient of determination (R^2) for the fitting was 0.9837, indicating an excellent fit, with a full width at half maximum of 0.07855 nm.
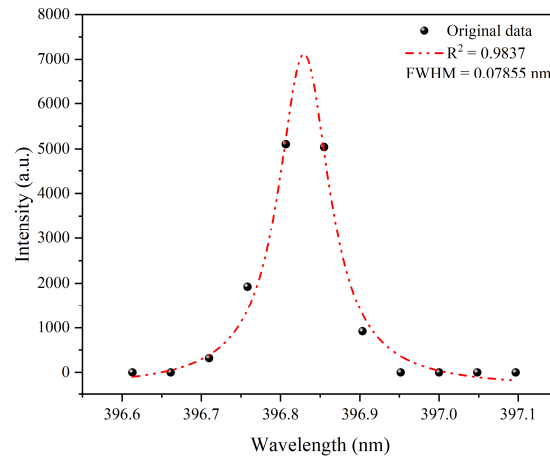
Figure 7. Lorentzian fitting of the Ca I 396.855 nm spectral line.

The electron collision coefficient for the Ca I 396.855 nm spectral line can be obtained from a database [29]. The calculated electron density for this test was 2.424×10^{21} cm^{-3}. According to the McWhirter criterion [30],

$$n_e \geq 1.6 \times 10^{12} \Delta E^3 T^{1/2} \text{cm}^{-3} \tag{4}$$

In this context, n_e represents the electron density; ΔE denotes the energy level difference of particle transitions in the plasma (with a value of 3.123 eV in this case), and the value here is 3.123 eV; and T indicates the plasma temperature. When inequality holds, it can be considered that the plasma is in a state of local thermodynamic equilibrium. Thus, it is understood that the calculation results conformed to the conditions of local thermodynamic equilibrium.

LIBS tests were conducted on the samples with a delay time of 1 μs and a single-pulse laser energy of 75 mJ. Under these conditions, spectra with strong line intensities were obtained. A total of 250 tests was performed on the samples, and the plasma temperature of the samples varied with the number of laser pulses, as shown in Figure 8, while the electron density of the samples varied with the number of laser pulses, as illustrated in Figure 9. Due to the fluctuations in LIBS testing and calculation errors, a Savitzky–Golay filter was applied to the raw plasma temperature and electron density data to better identify the trends in plasma parameter variations. This filter can smooth the data without distorting the underlying trends. The plasma parameters (temperature and electron density) gradually stabilized as the number of laser pulses increased. This is primarily attributed to the progressive formation of ablation craters and changes in the interaction mechanism between the laser and the material. In the initial stage, due to the relatively smooth surface of the material, the laser energy can efficiently act on the material's surface, generating high-temperature, high-density plasma. However, as the number of laser pulses increases, the ablation craters deepen, altering the plasma's expansion and cooling processes and imposing constraints on its behavior. These constraints slow down the random diffusion of the plasma, leading to a gradual stabilization of its temperature and electron density. As the plasma parameters stabilize, the fluctuations in LIBS signals decrease, thereby improving the repeatability and reliability of the spectral signals. Based on this, the Levenberg–Marquardt optimization algorithm was employed, and an exponential function was selected to fit the curves of plasma parameters as a function of the number of laser pulses, excluding the first 25 data points for plasma temperature fitting. The fitting results indicate a good fit, with a coefficient of determination of 0.9848 for the plasma temperature

as a function of the number of laser pulses, and a coefficient of determination of 0.9416 for the electron density as a function of the number of laser pulses.
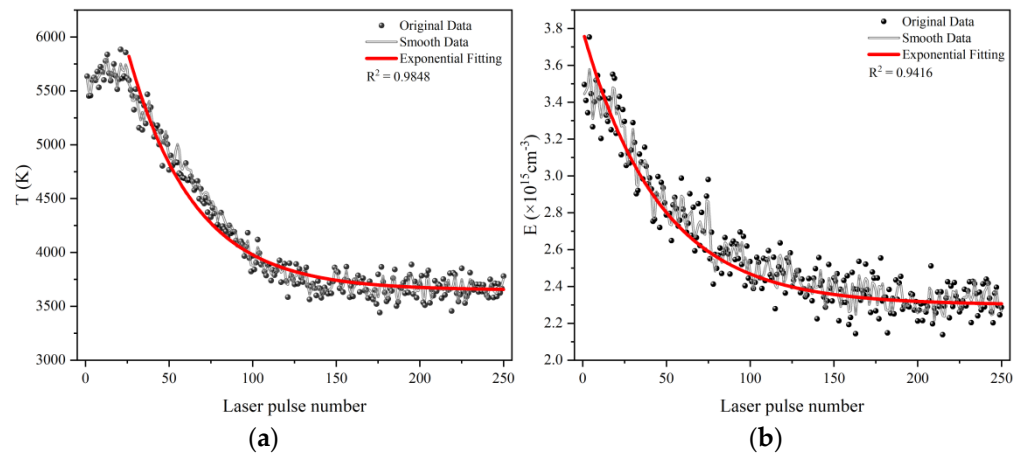

Figure 8. Results of plasma parameter calculations: (**a**) variation curve of plasma temperature with the number of laser pulses; (**b**) variation curve of electron density with the number of laser pulses.
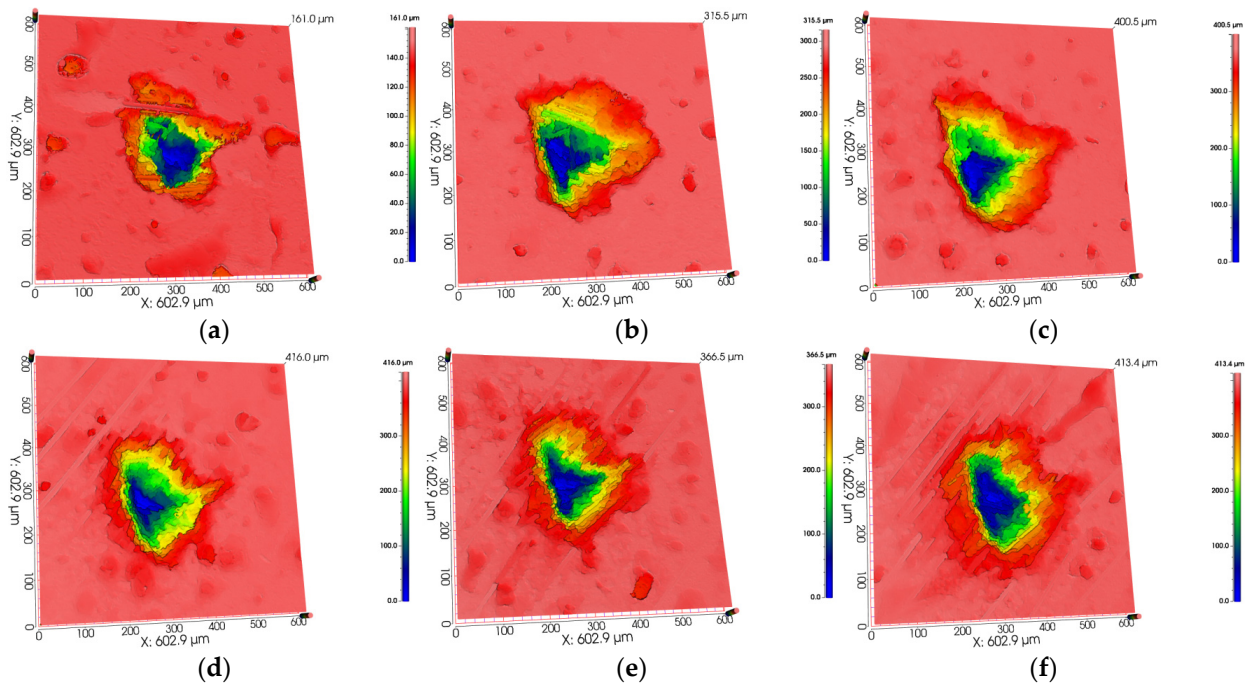

Figure 9. Confocal microscope test results: (**a–f**) show the laser ablation morphology at pulse counts of 10, 50, 100, 150, 200, and 250, respectively.

Through fitting analysis, it was found that the plasma temperature exhibits an asymptotic trend with varying laser pulse counts, indicating that the plasma temperature stabilizes after a certain number of laser pulses. Similarly, the electron density of the sample also gradually stabilizes with increasing laser pulse counts. The stability of the plasma characteristic parameters reflects the stability of the plasma itself, which in turn indicates the stability of the LIBS testing signal. This study hypothesizes that when the difference between the values of plasma parameters (temperature and electron density) and the asymptotic values of an exponential function is within 1% of the difference between the maximum and minimum values of the plasma parameters, the plasma state can be considered stable. Based on this hypothesis, we can conclude that the plasma temperature reached a stable state after the 187th pulse, while the electron density stabilized after the 192nd pulse.

3.2. Ablation Characteristics

To determine the relationship between the number of laser pulses and the size of the pits, this study utilized a laser confocal microscope to investigate the ablation characteristics of SMC materials, specifically the ablation depth and ablation area in relation to the number of laser pulses. The number of laser pulses tested was 10, 50, 100, 150, 200, and 250, with the results from the laser confocal microscope shown in Figure 9. It was observed that the ablation morphology was irregular, exhibiting conical pits. The formation of this ablation morphology was due to multiple factors. The test material was composed of resin and fiberglass, and the difference in ablation thresholds between the two materials led to an irregular ablation morphology. Additionally, fluctuations in laser parameters can affect the uniformity of energy distribution, further contributing to the irregularity of the ablation pit shapes.

By performing a linear fit on the average ablation depth, average ablation area, and the number of laser pulses, the relationship between these variables can be established. The coefficient of determination (R^2) for the two sets of fits was 0.818 and 0.855, indicating a strong correlation between ablation depth and ablation area with the number of laser pulses. The specific fitting formulas are as follows:

$$y = 0.942x + 176.6$$
$$z = 0.000731x + 0.260$$

(5)

In this context, x represents the number of laser pulses, y denotes the average ablation depth measured in micrometers (μm), and z indicates the average ablation area expressed in square millimeters (mm^2). From this, it can be roughly estimated that, for SMC materials, when the average ablation area is between 0.397 mm^2 and 0.443 mm^2, and the average ablation depth is between 0.353 mm and 0.412 mm, the plasma temperature remains stable. Additionally, when the average ablation area is between 0.400 mm^2 and 0.443 mm^2, and the average ablation depth is between 0.357 mm and 0.412 mm, the electron density is also stable. If we take the average values of these two parameters, the plasma state stabilizes when the average ablation area of the ablation pit is between 0.399 mm^2 and 0.443 mm^2, and the average ablation depth ranges from 0.355 mm to 0.412 mm.

3.3. Signal Stability Enhancement

This study selected four typical spectral lines from different elements (Ti II 334.940 nm, K II 338.486 nm, Ca I 445.478 nm, and Fe I 455.445 nm) and compared the RSD of the spectral line intensities under four different conditions, as shown in Figure 10. The first condition, labeled S1, involved spectral measurements obtained from 1 to 20 laser pulse tests. The second condition, S2, comprised spectral tests corresponding to the 187th to 207th laser pulses, taken after the plasma temperature stabilized. The third condition, S3, included spectral measurements from the 192nd to 212th laser pulses, taken once the electron density had stabilized. The fourth condition, S4, represented spectral tests derived from an average of 189 to 209 laser pulses, corresponding to stabilized plasma parameters.

In this work, the RSD was used to describe the stability of LIBS test signals, and it is defined as follows:

$$RSD(\%) = \frac{SD}{Mean}$$

(6)

In this context, SD represents the standard deviation of the signal intensity measured multiple times for a specific spectral line of an element, while Mean represents the average signal intensity measured multiple times for the same spectral line. The RSD can be used to evaluate the stability of the signal intensity; the smaller the RSD, the lower the

degree of dispersion in the signal intensity obtained from multiple tests, indicating a higher repeatability and stability of the LIBS measurements.
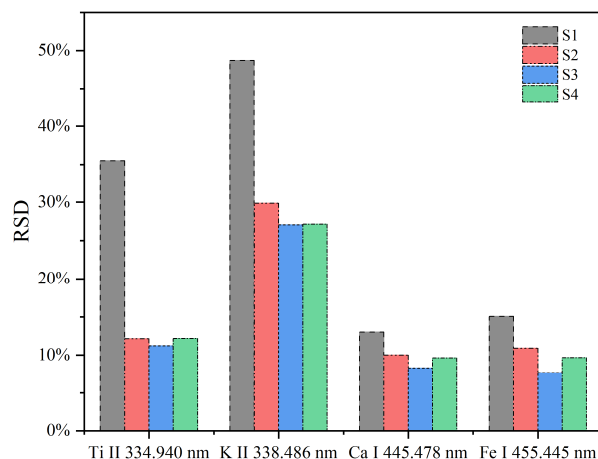

Figure 10. RSD of four spectral lines under different conditions.

Figure 10 shows the RSD results for the four spectral lines under these conditions. Specifically, in the S1 group, the RSD for Ti II 334.940 nm, K II 338.486 nm, Ca I 445.478 nm, and Fe I 455.445 nm was 35.49%, 48.7%, 13.02%, and 15.06% respectively. In S2, the RSD values were 12.13%, 29.86%, 10%, and 10.91%; for S3, they were 12.18%, 27.13%, 9.64%, and 9.68%; and in the S4 group, they were 11.22%, 27.06%, 8.3%, and 7.69%. The results indicate that the RSD of the four elemental spectral lines in S2, S3, and S4 significantly reduced compared to S1, with the greatest reduction observed for Ti II 334.940 nm. Although the RSD differences among S2, S3, and S4 were minimal, S3 provided the best improvement in test stability. Under the S3 dimensional conditions, the plasma temperature and electron density tend to stabilize, which is a key factor in improving the repeatability of LIBS test signals. The formation of ablation craters constrains the expansion and cooling processes of the plasma, reducing random diffusion and making its spatial distribution more uniform, thereby minimizing signal fluctuations. At the same time, stable craters ensure a more uniform interaction between the laser and the material, resulting in a higher consistency in the characteristics of the generated plasma.

Based on the RSD of spectral line intensities of four elements under different pulse counts, and considering the variations in laser ablation characteristic parameters, it can be approximated that when the ablation area of individual pits is between 0.400 mm^2 and 0.443 mm^2, and the ablation depth is between 0.357 mm and 0.412 mm, the pits impose a constraining effect on the plasma. This leads to the reflection of the plasma fundamental wave within the pits, thus stabilizing the plasma state, reducing signal fluctuations, and enhancing the stability of LIBS testing.

4. Conclusions

This study reflects the plasma state through characteristic parameters of the plasma and determines pit sizes based on the ablation features of the samples, thereby enhancing the stability of the LIBS testing. The plasma temperature and electron density were determined using a method that solves for multiple elements and spectral lines. Based on the variations in plasma temperature and electron density, the number of laser pulses required for the plasma state to stabilize was established. Using a laser confocal microscopy, the relationship between the ablation depth and ablation area with changes in the number of laser pulses was measured, allowing for the determination of the pit size corresponding to the number of laser pulses. We selected four typical elemental spectral lines: Ti II 334.940 nm, K II 338.486 nm, Ca I 445.478 nm, and Fe I 455.445 nm. By comparing the

relative standard deviation (RSD) of the intensities of the four elemental spectral lines at different pit sizes, it was ultimately determined that when the conical pit size is between 0.400 mm^2 and 0.443 mm^2, and the ablation depth is between 0.357 mm and 0.412 mm, the stability of the LIBS testing results showed significant improvement.

References

1. Kearton, B.; Mattley, Y. Sparking new applications. *Nat. Photonics* **2008**, *2*, 537–540. [CrossRef]
2. Harefa, E.; Zhou, W.D. Laser-Induced Breakdown Spectroscopy Combined with Nonlinear Manifold Learning for Improvement Aluminum Alloy Classification Accuracy. *Sensors* **2022**, *22*, 3129. [CrossRef] [PubMed]
3. Zheng, K.X.; Li, X.L.; Song, S.Z.; Gao, X. Discrimination of ginseng origin by using laser-induced breakdown spectrum and machine learning algorithms. *Microw. Opt. Technol. Lett.* **2023**, *65*, 1248–1254. [CrossRef]
4. Roh, S.B.; Park, S.B.; Oh, S.K. Development of intelligent sorting system realized with the aid of laser-induced breakdown spectroscopy and hybrid preprocessing algorithm-based radial basis function neural networks for recycling black plastic wastes. *J. Mater. Cycles Waste Manag.* **2018**, *20*, 1934–1949. [CrossRef]
5. Lian, Q.L.; Li, X.Y.; Lu, B.; Zhu, C.W.; Li, J.T.; Chen, J.J. Identification of Lung Tumors in Nude Mice Based on the LIBS With Histogram of Orientation Gradients and Support Vector Machine. *IEEE Access* **2023**, *11*, 141915–141925. [CrossRef]
6. Poggialini, F.; Fiocco, G.; Campanella, B. Stratigraphic analysis of historical wooden samples from ancient bowed string instruments by laser induced breakdown spectroscopy. *J. Cult. Herit.* **2020**, *44*, 75–284. [CrossRef]
7. Shen, J.X.; Liu, L.; Chen, Y.; Sun, Y.; Lin, W. Geochemical and Biological Profiles of a Quartz Stone in the Qaidam Mars Analog Using LIBS: Implications for the Search for Biosignatures on Mars. *ACS Earth Space Chem.* **2022**, *6*, 2595–2608. [CrossRef]
8. Zhu, Z.F.; Wang, X.Y.; Wu, T.F.; Li, Z.S.; Gao, E.R.; Gao, Q.; Li, B. Effect of gas temperature on composition concentration measurements by laser-induced breakdown spectroscopy. *J. Anal. At. Spectrom.* **2023**, *38*, 382–390. [CrossRef]
9. Liu, J.C.; Hou, Z.Y.; Wang, Z. The influences of ambient humidity on laser-induced breakdown spectroscopy. *J. Anal. At. Spectrom.* **2023**, *38*, 2571–2580. [CrossRef]
10. Karki, V.; Sarkar, A.; Singh, M.; Maurya, G.S.; Kumar, R.; Rai, A.K.; Aggarwal, S.K. Comparison of spectrum normalization techniques for univariate analysis of stainless steel by laser-induced breakdown spectroscopy. *Pramana J. Phys.* **2016**, *86*, 1313–1327. [CrossRef]
11. Zhou, Y.; Sun, L.; Li, Y. Combination of the internal standard and dominant factor PLS for improving long-term stability of LIBS measurements. *J. Anal. At. Spectrom.* **2024**, *39*, 1778–1788. [CrossRef]
12. Pan, C.Y.; Du, X.W.; An, N.; Zeng, Q.; Wang, S.B.; Wang, Q.P. Quantitative Analysis of Carbon Steel with Multi-Line Internal Standard Calibration Method Using Laser-Induced Breakdown Spectroscopy. *Appl. Spectrosc.* **2016**, *70*, 702–708. [CrossRef] [PubMed]
13. Cui, M.; Deguchi, Y.; Wang, Z. Enhancement and stabilization of plasma using collinear long-short double-pulse laser-induced breakdown spectroscopy. *At. Spectrosc.* **2018**, *142*, 14–22. [CrossRef]
14. Li, Y.; Zhao, J.; Cai, M.; Duan, H.; Li, Q.; Dai, Q.; Wu, R. Effect of argon on classification and identification of organics based on laser-induced breakdown spectroscopy. *Microw. Opt. Technol. Lett.* **2024**, *66*, e34340. [CrossRef]

15. Shen, X.K.; Sun, J.; Ling, H. Spatial confinement effects in laser-induced breakdown spectroscopy. In Proceedings of the International Congress on Applications of Lasers & Electro-Optics, LIA, Orlando, FL, USA, 29 October–1 November 2007.

16. Hou, Z.Y.; Wang, Z.; Lui, S.L. Improving data stability and prediction accuracy in laser induced breakdown spectroscopy by utilizing a combined atomic and ionic line algorithm. *J. Anal. Atom. Spectrom.* **2013**, *28*, 107–113. [CrossRef]

17. Wang, Z.; Li, L.Z.; West, L.; Li, Z.; Ni, W.D. A spectrum standardization approach for laser-induced breakdown spectroscopy measurements. *Spectrochim. Acta B* **2012**, *68*, 58–64. [CrossRef]

18. Elnasharty, I.Y.; Doucet, F.R.; Gravel, J.F.Y.; Bouchard, P.; Sabsabi, M. Double-pulse LIBS combining short and long nanosecond pulses in the microjoule range. *Acta Phys. Sin.* **2014**, *29*, 1660–1666.

19. Hussain, A.; Xun, G.; Asghar, H. Enhancement of Laser-induced Breakdown Spectroscopy (LIBS) Signal Subject to the Magnetic Confinement and Dual Pulses. *Opt. Spectrosc.* **2021**, *129*, 452–459. [CrossRef]

20. Jogi, I.; Ristkok, J.; Butikova, J.; Raud, J.; Paris, P. LIBS plasma in atmospheric pressure argon, nitrogen and helium: Spatio-temporal distribution of plume emission and Hα linewidth. *Nucl. Mater. Energy* **2023**, *37*, 101543. [CrossRef]

21. Song, Y.; Hou, Z.; Yu, X.; Yao, W.; Wang, Z. Exploring the impact mechanism of ambient gas properties on laser-induced breakdown spectroscopy to guide the raw signal improvement. *Anal. Chim. Acta* **2025**, *1335*, 343464. [CrossRef] [PubMed]

22. Wang, Y.; Jia, Y.; Gao, L. The effects of cavity diameter and material type of spatial confinement on intensity of laser-induced breakdown spectroscopy. *Phys. Scr.* **2023**, *98*, 015610. [CrossRef]

23. Li, C.; Xu, D.; Song, S. Enhancement of spectral line intensity and lifetime of femtosecond laser-induced Cu plasma in a cylindrical cavity. *Optik* **2022**, *271*, 170113. [CrossRef]

24. Shen, H.; Jian, H.; Zhen, H.; Yu, L.; Chen, H.; Tong, T.; Cui, X.; Wang, X. Laser-Induced Breakdown Spectroscopy Analysis of Sheet Molding Compound Materials. *Energies* **2024**, *17*, 2964. [CrossRef]

25. NIST Atomic Spectra Database Lines Form. Available online: https://physics.nist.gov/PhysRefData/ASD/lines_form.html (accessed on 26 October 2024).

26. Soumyashree, S.; Kumar, P. Effect of plasma temperature and electron number density on signal enhancement observed in nanoparticle enhanced LIBS. *J. Opt.* **2022**, *24*, 054008. [CrossRef]

27. Stetzler, J.; Tang, S.; Chinni, R.C. Plasma Temperature and Electron Density Determination Using Laser-Induced Breakdown Spectroscopy (LIBS) in Earth's and Mars's Atmospheres. *Atoms* **2020**, *8*, 50. [CrossRef]

28. Abdellatif, G.; Imam, H. A study of the laser plasma parameters at different laser wavelengths. *Spectrochim. Acta B* **2002**, *57*, 1155–1165. [CrossRef]

29. Database for "Stark" Broadening of Isolated Lines of Atoms and Ions in the Impact Approximation. Available online: http://stark-b.obspm.fr/index.php/home (accessed on 26 October 2024).

30. Zhao, X.X.; Luo, W.F.; He, J.F. Measurements of electron number density and plasma temperature using LIBS. In Proceedings of the International Symposium on Optoelectronic Technology and Application 2016, Beijing, China, 9–11 May 2016.